fibers

MDPI

Article

Short-Term Glucose Release from Ultrasound-Assisted Alkali-Pretreated Hemp Hurds Using Free and Magnetic Nanoparticle-Immobilised Cellulase

Ziningi Rosebud Myeni [1,*], Sani Gumede [2], Farai Dziike [1] and Nirmala Deenadayalu [1]

[1] Faculty of Applied Sciences, School of Chemistry, Durban University of Technology, Steve Biko Campus, Cnr Botanic Gardens & Steve Biko Roads, Durban 4001, KwaZulu-Nata, South Africa
[2] Technology Innovation Agency, Umbogintwini Industrial Complex, 1 Dickens Road, 28 Wharhist Street, Umbogintwini 4120, KwaZulu-Nata, South Africa
* Correspondence: 22383157@dut4life.ac.za

Highlights

What is the main finding?

- Cellulase immobilised on amine-functionalised magnetic nanoparticles achieved an immobilisation efficiency of 80.1 ± 0.6% and generated approximately 88–91% of the glucose produced by free cellulase during the seven-hour hydrolysis of pretreated hemp hurds.

What is the implication of the main finding?

- The magnetically recoverable cellulase retained approximately 64% of its initial hydrolytic performance after five reuse cycles, demonstrating its potential as a recoverable and reusable biocatalyst for lignocellulosic biomass conversion and sustainable biorefinery applications.

Abstract

The enzymatic conversion of lignocellulosic biomass (LB) into fermentable sugars is important for the development of sustainable biorefineries. This study investigated the immobilisation of *Trichoderma reesei* (*T. reesei*) cellulase on amine-functionalised magnetic nanoparticles (MNPs) and evaluated the resulting biocatalyst for the hydrolysis of pretreated hemp hurd (HH) biomass. Fourier transform infrared spectroscopy (FTIR) and scanning electron microscopy (SEM) provided evidence consistent with cellulase association with the nanoparticles, with the estimated dry-state particle diameter increasing from 22.4 ± 0.4 to 27.8 ± 0.3 nm after immobilisation. The selected immobilised catalyst loading produced approximately 89% of the total filter-paper assay response obtained with the selected free-enzyme loading, although this comparison was not normalised to protein content. During 7 h hydrolysis experiments, glucose production increased progressively for both enzyme forms. Across the tested enzyme dilutions, immobilised cellulase generated approximately 88–91% of the glucose produced by free cellulase. The immobilised enzyme also retained approximately 64% of its initial hydrolysis performance after five reuse cycles. These findings demonstrate the potential of magnetic cellulase nanobiocatalysts for recoverable and reusable hydrolysis of lignocellulosic biomass. However, further studies are required to determine protein-normalised activity, immobilisation efficiency, longer-term stability, process economics and industrial scalability.

Check for updates

Academic Editors: Izabela Betlej, Agnieszka Laskowska and Piotr Boruszewski

Received: 16 June 2026
Revised: 21 July 2026
Accepted: 3 August 2026
Published: 6 August 2026

Copyright: © 2026 by the authors. Licensee MDPI, Basel, Switzerland. This article is an open access article distributed under the terms and conditions of the Creative Commons Attribution (CC BY) license.

Keywords: HH; lignocellulose biomass; biomass valorisation; hemp biorefinery; immobilised cellulase; glucose

1. Introduction

The increasing demand for sustainable alternatives to fossil-derived resources has intensified interest in lignocellulosic biomass as a renewable feedstock for the production of biofuels, biochemicals, biomaterials and other value-added products [1]. Within the transition towards a circular bioeconomy, agricultural residues and industrial biomass by-products are increasingly being investigated as low-cost renewable feedstocks for waste-valorisation processes [2]. Industrial hemp (*Cannabis sativa* L.) is particularly attractive because of its rapid growth, high biomass productivity, relatively low agricultural input requirements and capacity to sequester carbon during cultivation [3].

Industrial hemp processing generates substantial quantities of HHs, the lignocellulosic inner core of the hemp stem. HHs constitute approximately 70–80% of the stem and typically contain 40–48% cellulose, 18–24% hemicellulose and 21–24% lignin [4]. Their substantial carbohydrate content makes them a potential renewable carbon source for biochemical conversion. The cellulose fraction can be hydrolysed into glucose, while hemicellulose provides additional carbohydrates that may support downstream microbial bioconversion processes [5]. HHs therefore represent a promising feedstock for integrated biorefinery applications.

The conversion of lignocellulosic biomass into fermentable carbohydrates generally involves feedstock preparation, pretreatment, enzymatic hydrolysis and fermentation [6,7]. Enzymatic hydrolysis is a critical stage because cellulolytic enzymes convert cellulose into glucose and soluble cello-oligosaccharides that can serve as carbon sources for microbial production systems [8]. However, cellulose is embedded within a structurally complex matrix of lignin and hemicellulose, which restricts enzyme accessibility and contributes to biomass recalcitrance [9]. Effective pretreatment is therefore required to disrupt the lignin–carbohydrate matrix and increase the accessibility of cellulose to cellulolytic enzymes [10].

Previous investigations of South African-grown HH demonstrated that the biomass contained a substantial polysaccharide fraction but exhibited a compact and relatively non-porous structure that could restrict enzyme penetration [11]. Subsequent evaluation of organosolvent, oxidative–alkaline and ultrasound-assisted alkaline pretreatments showed that ultrasound-assisted sodium hydroxide treatment produced the greatest structural disruption and retained a substantial proportion of the biomass polysaccharides [12]. FTIR and SEM analyses indicated reductions in lignin- and hemicellulose-associated features together with increased fibre disruption and surface accessibility. Based on these findings, ultrasound-assisted sodium hydroxide-pretreated HHs were selected as the substrate for the present enzymatic hydrolysis study.

Efficient cellulose hydrolysis generally requires the synergistic action of endoglucanases, exoglucanases or cellobiohydrolases, and β-glucosidases [13,14]. *Trichoderma reesei* is widely used as an industrial source of cellulolytic enzymes because of its capacity to secrete highly active cellulase preparations [15]. Nevertheless, the use of free cellulase may be constrained by limited enzyme recovery and reuse, non-productive interactions with residual biomass components, product inhibition and the cost associated with repeated enzyme addition [16–18].

Enzyme immobilisation has been investigated as a strategy for improving catalyst recovery, reuse and operational stability [19,20]. Magnetic nanoparticles are particularly suitable as immobilisation supports because of their high surface-area-to-volume ratio,

modifiable surface chemistry and responsiveness to an external magnetic field. These properties facilitate enzyme association with the support and enable rapid magnetic separation of the recovered catalyst from the reaction medium [21,22]. However, the catalytic performance of an immobilised preparation depends on several factors, including the support material, immobilisation chemistry, enzyme orientation, surface loading, aggregation behaviour and accessibility of the enzyme active sites.

Magnetic nanoparticle-associated cellulase has previously been investigated for the hydrolysis of different lignocellulosic substrates, including hemp-derived biomass. However, limited information is available on its short-term hydrolytic performance and reusability when applied to ultrasound-assisted sodium hydroxide-pretreated HH within a sequential valorisation pathway. The contribution of the present study therefore lies in integrating a previously optimised hemp hurd pretreatment process with a direct comparison of free and magnetically recoverable cellulase preparations under identical hydrolysis conditions.

The objective of this study was to prepare cellulase-associated amine-functionalised magnetic nanoparticles and evaluate their application in the enzymatic hydrolysis of pretreated HH. Specifically, the study determined protein loading and immobilisation efficiency, characterised cellulase association with the nanoparticle preparation, compared the filter-paper activity and glucose-producing performance of free and immobilised cellulase, calculated glucose yield and glucose-based glucan conversion, and evaluated recovery and reuse of the immobilised preparation over five consecutive hydrolysis cycles.

This study forms the third stage of a broader hemp hurd valorisation pathway comprising feedstock characterisation, pretreatment optimisation and enzymatic conversion. The glucose-containing hydrolysates generated during this stage may subsequently be evaluated as intermediate carbon streams for microbial bioconversion. Future work will investigate the integration of cellulolytic and polyhydroxyalkanoate biosynthetic pathways for consolidated bioprocessing and PHA/PHB production. Figure 1 summarises the progression of this broader research pathway.

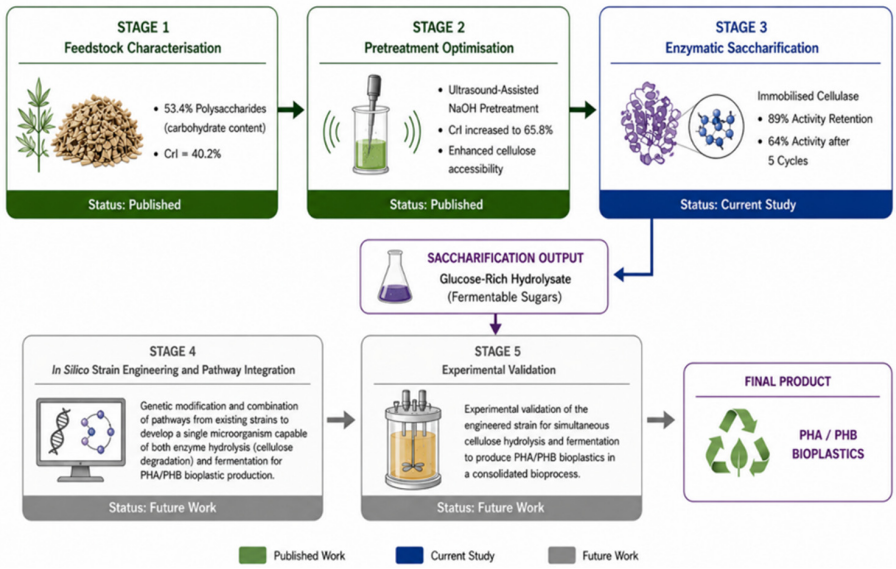

Figure 1. Process development pathway for the valorisation of HH towards PHA/PHB bioplastic production. Published studies established the physicochemical characteristics of HH and identified ultrasound-assisted NaOH pretreatment as the preferred strategy for improving cellulose accessibility. The current study investigates enzymatic hydrolysis using immobilised cellulase to produce a glucose-containing hydrolysate. Future work will focus on in silico strain engineering and pathway integration to develop a consolidated bioprocessing system capable of simultaneous cellulose degradation and fermentation for direct bioplastic production, followed by experimental validation of the engineered strain.

2. Materials and Methods

2.1. Preparation of Pretreated HH

The pretreated HH served as the substrate for all hydrolysis experiments. The HHs were sourced from a mixed cultivation of ARC-CAN-01 and ARC-CAN-03 cultivars in an approximately 50:50 ratio, during trial studies at Cedara, in collaboration with the Agricultural Research Council and the Department of Agriculture, Pietermaritzburg. Chemicals and reagents used were of analytical grade. The HHs were separated from the hemp stalk via manual decortication, ground and sieved through a 1 mm mesh, and particles passing through the sieve (<1 mm) were collected for all experiments. This process increased the surface area and ensured sample homogeneity. Five grams of HH was submerged in 50 mL of 2% (w/v) sodium hydroxide (NaOH) solution and subjected to ultrasound treatment using a Qsonica Q700 probe sonicator (maximum rated power 700 W, Qsonica, LLC, Newtown, CT, USA) equipped with a 12.7 mm titanium probe, operated at 60% amplitude for 30 min at 50 °C. The ultrasound-assisted NaOH treatment disrupted the biomass structure and improved cellulose accessibility. The final product was stored in an airtight container to prevent moisture uptake before use.

2.2. Activation and Immobilisation of Cellulase on Amine-Functionalised Magnetic Nanoparticles

Immobilisation of cellulase was conducted using amine-functionalised iron oxide nanoparticles (20 nm, 5 mg/mL). Although the magnetic nanoparticles were supplied with surface amine functionalities, Sulfo-SMCC was used as a heterobifunctional crosslinker to introduce maleimide groups onto the nanoparticle surface. These maleimide groups were intended to react with accessible sulfhydryl groups on the cellulase preparation, where such groups were present and sterically available under the conjugation conditions. The number of accessible thiol groups in the commercial cellulase preparation was not quantified before conjugation. Therefore, maleimide–thiol coupling is presented as the intended reaction pathway rather than as a quantitatively verified binding mechanism. A 0.25 mL aliquot of the nanoparticle suspension was combined with 0.25 mL of coupling buffer and activated by adding 0.038 mL of Sulfo-SMCC solution (10 mg/mL in DMSO). The mixture was incubated for 1 h at room temperature with continuous mixing to promote amide bond formation between NHS esters and surface amines. The activated nanoparticles were purified using a NAP-10 desalting column equilibrated with coupling buffer, and the eluted fraction (1.5 mL) was immediately mixed with 0.25 mL of the commercial cellulase preparation. The conjugation procedure was based on the potential reaction between nanoparticle-bound maleimide groups and accessible sulfhydryl groups within the cellulase preparation; however, the concentration of these groups was not independently determined. The conjugation reaction was allowed to proceed for 4 h at room temperature with gentle agitation. The reaction was quenched by adding 0.05 mL of quenching buffer and incubating for 30 min. Conjugated nanoparticles were purified using a SuperMag Multitube Separator (Ocean NanoTech, LLC, San Diego, CA, USA) for 8–12 h with repeated washing in storage buffer to remove unbound enzyme. The final immobilised cellulase preparation was stored at 4 °C until use.

Following conjugation, the particles were magnetically separated and washed repeatedly to remove loosely associated enzyme. These washing steps reduced the presence of unbound protein but could not distinguish covalently attached enzyme from protein retained through strong physical adsorption, electrostatic interactions or other non-covalent forces.

2.3. Determination of Protein Loading and Immobilisation Efficiency

Protein concentration was determined using a matrix-matched Bradford assay with bovine serum albumin as the calibration standard. Protein measurements were performed for the initial cellulase solution introduced into the immobilisation reaction, the post-conjugation supernatant and the combined wash fractions. Samples containing nanoparticles were magnetically clarified before absorbance measurement to minimise interference from suspended particles. Appropriate buffer, reagent and nanoparticle blanks were included.

Three independent immobilisation preparations were analysed. The mass of protein associated with the recovered MNP preparation was calculated by protein mass balance (Equation (1)):

$$M_{iassociated} = M_{initial} - M_{supernatant} - M_{wash} \quad (1)$$

Immobilisation efficiency was calculated using Equation (2) as follows:

$$\text{Immobilisation efficiency } \% = (M_{associated}/M_{initial}) \times 100 \quad (2)$$

Protein loading was calculated relative to the mass of MNPs used according to Equation (3):

$$\text{Protein loading } (mg.g^{-1}) = M_{associated}\ (mg)/M_{MNP}\ (g) \quad (3)$$

Results are reported as mean ± standard deviation from three independently prepared immobilisation batches.

2.4. FTIR Characterisation of Cellulase Association with MNPs

Fourier transform infrared (FTIR) spectra of free cellulase, nanoparticles, and cellulase–nanoparticle conjugates were collected using a Shimadzu IRSpirit FTIR equipped with an attenuated total reflectance (ATR) accessory. Spectra were recorded over 4000–400 cm^{-1} at 4 cm^{-1} resolution with 32 scans per sample.

The appearance of the Amide I and Amide II bands in the cellulase-associated MNP spectrum was interpreted as qualitative evidence consistent with protein association with the nanoparticle preparation.

2.5. Surface Morphology Using SEM

The surface morphology and dry-state particle size of the amine-functionalised MNP were examined before and after cellulase immobilisation using a scanning electron microscope (JEOL Ltd., Akishima, Japan). The dried nanoparticle samples were mounted on aluminium stubs using conductive carbon tape and prepared for SEM imaging. The samples were examined at accelerating voltages of 10 kV. One representative SEM micrograph was obtained for each preparation.

Indicative dry-state particle diameters were estimated from the SEM micrographs using ImageJ software (National Institutes of Health, Bethesda, MD, USA; Fiji/ImageJ version 1.54). Each image was calibrated using its corresponding scale bar, and the diameters of clearly distinguishable particle features within the field of view were measured. A total of n = 10 particle features were measured for each preparation. Large agglomerates and features with poorly defined boundaries were excluded from the primary-particle diameter estimation but were considered qualitatively when assessing particle aggregation. The mean dry-state particle diameter and standard deviation were calculated from the individual measurements within each micrograph. Because only one microscopic field was analysed for each preparation, the reported standard deviations represent within-image particle-size variation rather than variability among independently prepared samples or

multiple fields of view. The values should therefore be regarded as indicative image-based dry-state estimates and not as comprehensive particle-size distributions.

2.6. Determination of Enzyme Activity

The activity of free and immobilised cellulase was determined using the filter-paper unit (FPU) assay described by Ghose. Whatman No. 1 filter-paper strips (50 mg) served as the cellulose substrate. After incubation under standard assay conditions for 30 min, released reducing sugars were quantified using the dinitrosalicylic acid (DNS) assay, with glucose as the standard reference, measuring absorbance at 540 nm. Enzyme activity (FPU/mL) was calculated according to Ghose's equation, and relative activity was determined by comparing immobilised and free cellulase activities. Enzyme activity was expressed as FPU mL^{-1} based on the amount of enzyme required to release 2 mg of reducing sugar from Whatman No. 1 filter paper. The cellulase activity was calculated using the modified filter-paper activity assay based on the Ghose procedure. The dilution that released approximately 2 mg of glucose from 50 mg Whatman No. 1 filter paper after 30 min was used to calculate cellulase activity. Under the assay conditions employed, the free cellulase preparation exhibited an activity of 0.37 U, while immobilised cellulase exhibited an activity of 0.33 U. Relative activity was calculated using Equation (4):

$$\text{Relative Filter Paper Assay response (\%)} = A_{\text{Immobilised}}/A_{\text{free}} \times 100 \quad (4)$$

The Ghose assay measures cellulolytic activity using pure cellulose (Whatman No. 1 filter paper), but it does not capture the structural complexity of LB such as HH. Nonetheless, the assay provides a reliable baseline for comparing free and immobilised enzymatic systems.

2.7. Enzymatic Hydrolysis

Enzymatic hydrolysis experiments were conducted in batch mode using pretreated HHs at fixed substrate loading, temperature and pH. Hydrolysis reactions were performed in 50 mM citrate buffer (pH 4.8) with 400 mg of pretreated hurds (2% w/v) in a total volume of 20 mL. Free or immobilised cellulase was added at enzyme loadings corresponding to Ghose assay dilution factors of 2.5, 5, 10, 15 and 20. Reactions were incubated at 50 °C and 150 rpm for 7 h. Samples were withdrawn at hourly intervals, immediately heated to 100 °C for 5 min to deactivate enzymes, centrifuged and stored at 4 °C prior to glucose analysis. Hydrolysis was performed at pH 4.8 and 50 °C, conditions commonly reported as optimal for cellulase preparations derived from *T. reesei* [23].

The apparent average glucose release rates were calculated for descriptive comparison of the free and immobilised cellulase preparations. The experiments were not designed for determination of Michaelis–Menten kinetic parameters because initial reaction rates were not measured over a range of substrate concentrations. Consequently, K_m, $V_{\max}$ and k_{cat} were not calculated.

2.8. Glucose Quantification

Glucose released during hydrolysis was quantified by HPLC using an Aminex HPX-87H column with 5 mM H_2SO_4 as the mobile phase at 0.6 mL/min and 60 °C. Detection was performed using a refractive index detector and an injection volume of 10 µL. Glucose concentrations were calculated using external calibration with analytical standards.

2.8.1. Glucose Concentration

Glucose concentration was obtained directly from the HPLC calibration curve using Equation (5):

$$\text{Glucose concentration (g/L)} = (A - b)/m \quad (5)$$

where A is peak area, m is the calibration slope and b is the intercept of the glucose calibration curve.

2.8.2. Glucose Yield in Equation (6)

$$\text{Glucose yield (g/g LB)} = \text{Glucose produced (g)/Initial dry LB (g)} \quad (6)$$

2.8.3. Glucan Conversion and Partial Biomass-to-Glucose Mass Balance

The glucan content of the pretreated HH was determined from three independent compositional analyses and expressed as a percentage of dry biomass. The measured glucan content was 42.6%.

The initial glucan mass in each hydrolysis reaction was calculated using Equation (7) as follows:

$$M_{glucan} = M_{biomass} \times f_{glucan} \quad (7)$$

where $M_{biomass}$ is the initial dry mass of pretreated HH and f_{glucan} is the experimentally determined glucan fraction.

Glucose mass was calculated from the measured glucose concentration and the hydrolysis reaction volume using Equation (8):

$$M_{glucose} = C_{glucose} \times V \quad (8)$$

Glucose yield relative to the initial dry biomass was calculated using Equation (9) as follows:

$$\text{Glucose yield (g/g)} = M_{glucose}/M_{biomass} \quad (9)$$

Glucan conversion was calculated by applying an anhydro correction factor of 0.90 to convert measured glucose mass to its equivalent glucan mass using Equation (10):

$$\text{Glucan conversion (\%)} = (M_{glucose} \times 0.90)/M_{glucan} \times 100 \quad (10)$$

The calculation represents conversion of the initial glucan fraction to quantified glucose during the seven-hour hydrolysis period. Because other soluble sugars, residual insoluble carbohydrates and processing losses were not quantified, the calculation constitutes a partial biomass-to-glucose mass balance rather than a complete carbohydrate mass balance.

2.8.4. Apparent Average Glucose Release Rate

The apparent average glucose release rate was calculated by dividing the glucose concentration measured at the end of the seven-hour hydrolysis period by the total reaction time using Equation (11):

$$\text{Apparent average glucose release rate} = (C_{7h} - C_{0h})/7\ \text{h} \quad (11)$$

where C_{7h} and C_{0h} represent the glucose concentrations measured at seven hours and at the beginning of hydrolysis, respectively. Because the initial glucose concentration was zero under the experimental conditions, the calculation was equivalent to dividing the final glucose concentration by seven hours. These values were used only for descriptive comparison of the free and immobilised cellulase preparations. They do not represent initial reaction rates, kinetic rate constants or Michaelis–Menten parameters.

The analytical method was calibrated specifically for glucose, which was selected as the principal response variable for comparing the short-term hydrolytic performance of the free and immobilised cellulase preparations. Other soluble carbohydrates, including cellobiose, cello-oligosaccharides and hemicellulose-derived monosaccharides, were not

quantified because authentic standards for these compounds were not included in the calibration procedure. The reported concentrations therefore represent glucose only and should not be interpreted as total soluble sugar concentration.

2.9. Reusability Testing of Immobilised Cellulase of Immobilised Cellulase

Reusability tests were conducted by recovering immobilised cellulase magnetically after each hydrolysis cycle, washing the particles with citrate buffer and re-introducing them into fresh reactions under identical conditions. Five consecutive cycles were performed. Residual hydrolytic performance (%) was calculated by comparing glucose production in each cycle with that measured in the first cycle. All enzymatic activity, hydrolysis and reusability experiments were performed in triplicate. Results are reported as mean ± standard deviation (SD) of three independent experiments.

2.10. Statistical Treatment

All enzyme-activity, hydrolysis and reusability experiments were performed as three independent experiments. Results are presented as mean ± standard deviation (n = 3), and standard deviations are displayed as error bars in the corresponding figures. The study was designed as a descriptive laboratory-scale comparison of free and immobilised cellulase under identical experimental conditions. Accordingly, comparisons were based on mean values, standard deviations and relative performance. Formal inferential statistical testing was not performed, and no differences are interpreted as statistically significant.

3. Results and Discussion

3.1. Protein Loading and Immobilisation Efficiency

Quantification of protein before and after conjugation provided a mass-balance estimate of the amount of cellulase associated with the magnetic nanoparticle preparation. The initial cellulase solution contained 0.0402 ± 0.0004 mg protein per preparation. Following conjugation and magnetic separation, 0.0065 ± 0.0003 mg was detected in the post-conjugation supernatant and 0.0015 ± 0.0002 mg was recovered in the combined wash fractions. The calculated quantity of protein associated with the recovered MNPs was therefore 0.0322 ± 0.0005 mg per preparation.

Based on the initial quantity of protein introduced, the immobilisation efficiency was 80.1 ± 0.6%. This produced a protein loading of 25.7 ± 0.4 mg protein g^{-1} MNP. These results quantitatively demonstrate that most of the protein introduced during the conjugation step was retained in the recovered nanoparticle preparation.

Immobilisation efficiency describes the proportion of the supplied protein associated with the recovered nanoparticle preparation. The approximately 80% immobilisation efficiency is therefore a protein mass-balance measurement. By contrast, the selected immobilised catalyst loading produced approximately 89% of the total filter-paper assay response obtained using the selected free-enzyme loading. Because the two preparations were compared on different loading bases, the 89% value should not be interpreted as protein-normalised activity retention.

The protein mass balance results are summarised in Table 1. These results mass balance do not establish that all retained protein was attached through Sulfo-SMCC-mediated covalent bonds. A proportion of the measured protein may have remained associated through physical adsorption, electrostatic interactions or other non-covalent forces. Nevertheless, the low protein quantities detected in the supernatant and wash fractions indicate substantial protein association with the recovered MNP preparation. Confirmation of the relative contributions of covalent attachment and physical adsorption would require crosslinker-free controls and protein-leaching measurements.

Table 1. Protein loading and immobilisation efficiency of cellulase associated with amine-functionalised MNPs.

Parameter	MEAN ± SD	UNIT
Initial Protein Introduced	0.0402 ± 0.0004	mg per preparation
Protein In Post-Conjugation Supernatant	0.0065 ± 0.0003	mg per preparation
Protein In Combined Wash Fractions	0.0015 ± 0.0002	mg per preparation
Calculated MNP-Associated Protein	0.0322 ± 0.0005	mg per preparation
Immobilisation Efficiency	80.1 ± 0.6	%
Protein Loading	25.7 ± 0.4	mg protein g^{-1} MNP

3.2. FTIR Evidence of Cellulase Association with MNPs

FTIR spectroscopy was used to evaluate spectral changes consistent with cellulase association with the amine-functionalised nanoparticles as shown in Figure 2. FTIR analysis showed spectral changes consistent with protein association with the functionalised MNP preparation through the appearance of characteristic amide bands. However, FTIR provides qualitative rather than quantitative evidence of enzyme immobilisation. Quantitative protein mass balance demonstrated an immobilisation efficiency of 80.1 ± 0.6% and a protein loading of 25.7 ± 0.4 mg protein g^{-1} MNP, complementing the qualitative FTIR and SEM evidence of cellulase association with the nanoparticle preparation.

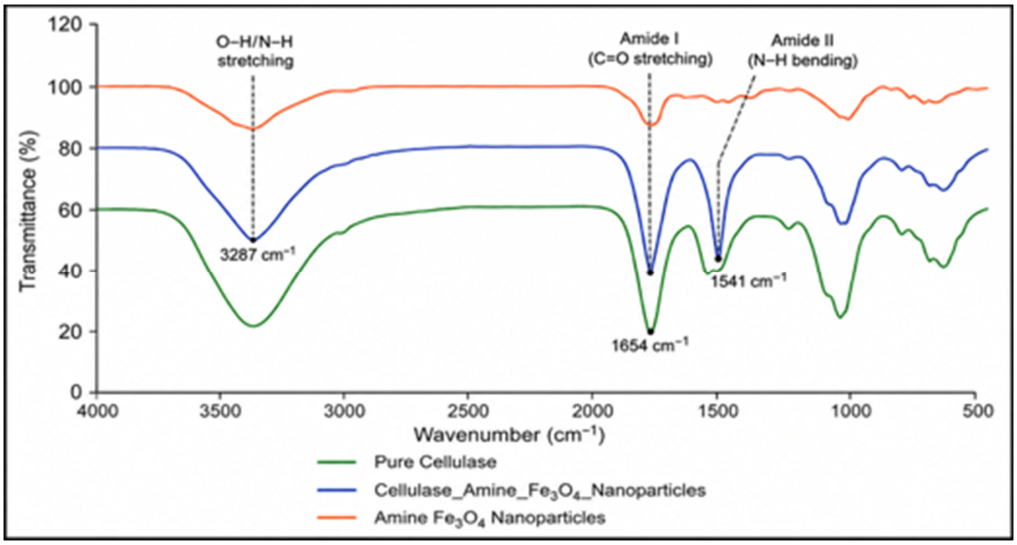

Figure 2. FTIR spectra of free cellulase, amine-functionalised magnetic nanoparticles and cellulase-associated magnetic nanoparticles. The appearance of Amide I and Amide II bands in the cellulase-associated MNP spectrum is consistent with the presence of protein-associated material following the immobilisation procedure. FTIR was used as qualitative supporting evidence and does not quantify protein loading or distinguish Sulfo-SMCC-mediated covalent coupling from physical adsorption or other non-covalent interactions.

The FTIR spectrum of free cellulase displayed several characteristic protein bands (Table 2), such as a broad band at 3200–3400 cm^{-1} for O–H and N–H stretching, an Amide I band at 1650 cm^{-1} (C=O stretching) and an Amide II band near 1540 cm^{-1}. Amine-functionalised nanoparticles showed bands for surface amine groups, including N–H stretching around 3300–3500 cm^{-1}. After conjugation, the FTIR spectrum indicated distinct changes: the appearance of Amide I and II bands at 1650 and 1540 cm^{-1} was consistent with protein association, while shifts and intensity reductions pointed to interactions between the enzyme and amine groups. The observed spectral changes are consistent with

protein association with the functionalised nanoparticle surface following the Sulfo-SMCC-mediated immobilisation procedure. However, the spectra do not independently confirm that maleimide–thiol coupling occurred.

Table 2. Characteristic FTIR absorption bands associated with cellulase and amine-functionalised magnetic nanoparticles.

Sample	Wavenumber (cm^{-1})	Functional Group	Interpretation
Free cellulase	~1654	Amide I (C=O stretch)	Protein backbone
Free cellulase	~1541	Amide II (N–H bend)	Protein backbone
NH_2-MNPs	~3287	N–H stretching	Amine groups
Cellulase–NH_2-MNPs	~1654	Amide I	Protein-associated amide band
Cellulase–NH_2-MNPs	~1541	Amide II	Protein-associated amide band

The appearance of the Amide I and Amide II bands in the cellulase–MNP spectrum provides qualitative evidence that material associated with protein was present on the nanoparticle surface. However, these spectral features do not establish the quantity of cellulase attached or independently confirm the chemical nature of the attachment. The observed changes in peak position and intensity may reflect several overlapping effects, including interactions between enzyme functional groups and the activated nanoparticle surface, changes in the local hydration environment, and possible conformational rearrangement of the protein following surface association. Depending on the orientation of individual cellulase molecules, these interactions could leave the catalytic regions accessible or partially restrict substrate access to the active sites.

The intended Sulfo-SMCC coupling reaction provides a chemically plausible pathway for maleimide–thiol conjugation; nevertheless, the number of accessible sulfhydryl groups in the commercial cellulase preparation was not determined. In addition, no desorption control, crosslinker-free adsorption control or protein-leaching measurement was performed. A contribution from physical adsorption or other non-covalent interactions therefore cannot be excluded. The FTIR results are therefore interpreted as evidence consistent with cellulase association with the functionalised MNPs rather than definitive proof of exclusively covalent immobilisation. Confirmation of the binding mechanism would require complementary measurements such as accessible thiol quantification, protein loading, immobilisation efficiency and enzyme-leaching analysis.

Cellulase from *T. reesei* was immobilised on activated magnetic nanoparticles via covalent binding, achieving up to 94% protein binding confirmed by FTIR [24]. Cellulase produced by *Aspergillus fumigatus* JCF was successfully immobilised onto MnO_2 nanoparticles, enhancing its activity and stability, with FTIR confirming the characteristics of the MnO_2 nanoparticles and the cellulase-bound variants [25].

3.3. SEM Analysis

SEM was used to compare the surface morphology of the amine-functionalised MNPs before and after cellulase immobilisation. As shown in Figure 3, both preparations consisted of approximately spherical nanoscale features arranged within larger agglomerated structures. The amine-functionalised MNPs had an indicative dry-state diameter of 22.4 ± 0.4 nm, whereas the cellulase-associated MNPs had an indicative diameter of 27.8 ± 0.3 nm. This represents an apparent increase of approximately 5.4 nm following the immobilisation procedure. The post-immobilisation sample was visually less uniform and had a more clustered morphology appearance.

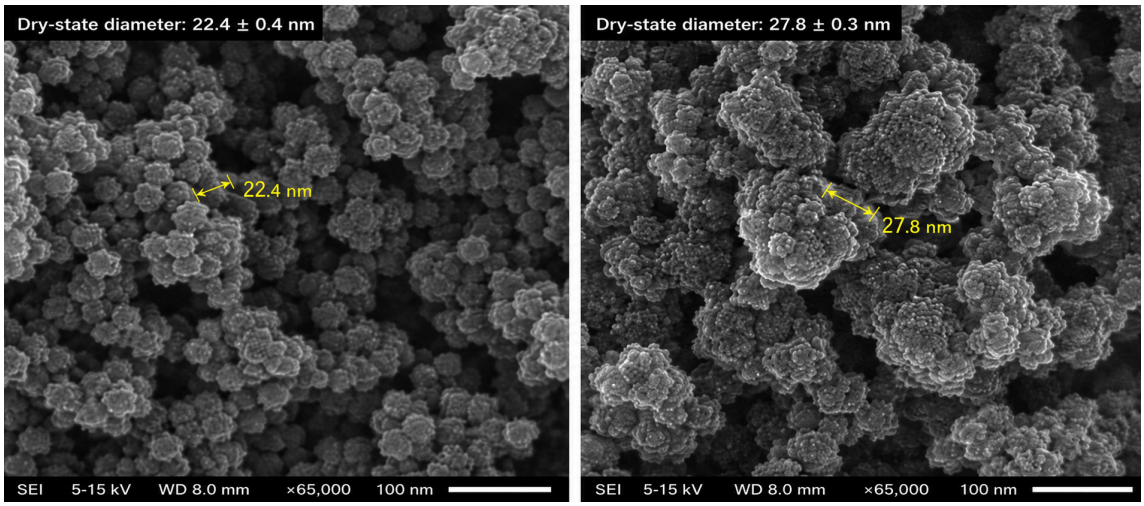

(**A**) (**B**)

Figure 3. SEM micrographs of (**A**) amine-functionalised MNPs before cellulase immobilisation and (**B**) cellulase-associated MNPs after the immobilisation procedure, obtained at an accelerating voltage of 5–15 kV and a magnification of 65,000×. Scale bar = 100 nm. The indicative dry-state particle diameter increased from 22.4 ± 0.4 nm to 27.8 ± 0.3 nm. The apparent increase and altered aggregation are consistent with the presence of surface-associated material after the immobilisation procedure but do not independently demonstrate a uniform enzyme coating or covalent attachment. Because one micrograph was analysed for each preparation, the values represent indicative image-based estimates rather than complete particle-size distributions.

The apparent increase in dry-state diameter is consistent with the presence of additional surface-associated material after exposure of the activated MNPs to cellulase. However, the increase cannot be attributed exclusively to the formation of a uniform enzyme coating. Changes in nanoparticle aggregation during conjugation, washing, magnetic separation and drying may also have contributed to the measured difference. Magnetic particle–particle interactions and sample dehydration during SEM preparation may promote agglomeration, making it difficult to distinguish isolated primary particles from closely associated particle clusters.

The observed aggregation may also have implications for catalytic performance. Closely packed particles could reduce the effective surface area available for enzyme–substrate contact, create steric crowding between neighbouring enzyme molecules and restrict the orientation of some immobilised cellulase molecules. Aggregated structures may additionally increase the diffusion distance required for insoluble cellulose chains, soluble oligosaccharides and glucose to move toward or away from enzyme-containing regions, thereby contributing to local mass-transfer resistance. Conversely, cellulase molecules positioned on exposed outer surfaces may remain accessible to the substrate and retain substantial catalytic activity. The SEM observations therefore provide morphological evidence consistent with changes following immobilisation but do not establish the extent of enzyme coverage, active-site orientation or the chemical nature of enzyme attachment.

Only one SEM micrograph was analysed for each preparation. The reported standard deviations therefore describe the variation among measurable particles within the selected images and do not represent variation among independently prepared samples or multiple microscopic fields. The diameter values should consequently be regarded as indicative dry-state estimates rather than complete particle-size distributions. Complementary techniques such as DLS, TEM and zeta-potential measurements would be required to evaluate hydrodynamic size, aggregation behaviour and surface changes more comprehensively.

3.4. Filter-Paper Activity

The catalytic responses of the free and immobilised cellulase preparations were evaluated using the Ghose filter-paper assay with Whatman No. 1 filter paper as the cellulose substrate [26]. The assay reflects the combined activity of the cellulase components: endoglucanases generate new cellulose-chain ends, cellobiohydrolases or exoglucanases release soluble cello-oligosaccharides, and β-glucosidase converts the soluble products to glucose. The selected free-cellulase dilution of 1:40 released 2.00 ± 0.08 mg of reducing sugars, expressed as glucose equivalents, within 30 min, corresponding to a total assay activity of 0.37 ± 0.02 U. The selected immobilised catalyst loading of 20 mg released 1.80 ± 0.10 mg and produced a total assay activity of 0.33 ± 0.02 U, as presented in Table 3.

Table 3. Ghose assay activity data.

Enzyme	Dilution/Mass	Glucose Released (mg)	Activity (U)	Relative Filter-Paper Assay Response (%)
Free cellulase	1:40	2.00 ± 0.08	0.37 ± 0.02	100 ± 4
Immobilised cellulase	20 mg	1.80 ± 0.10	0.33 ± 0.02	89 ± 5

Relative filter-paper assay response was calculated by expressing the total assay response of the selected immobilised catalyst loading as a percentage of that obtained using the selected free-enzyme loading. Because the preparations were compared on different loading bases, this percentage does not represent protein-normalised activity retention. Values represent mean ± SD (n = 3).

The immobilised catalyst therefore produced 89 ± 5% of the total filter-paper assay response obtained with the selected free-enzyme loading. This result confirms that the recovered nanoparticle-associated cellulase remained catalytically functional following the immobilisation procedure. However, the free and immobilised preparations were evaluated on different loading bases—enzyme dilution and catalyst mass, respectively. The 89% value therefore represents a relative filter-paper assay response and not protein-normalised activity retention, intrinsic activity preservation or immobilisation efficiency. It should consequently not be compared directly with activity-retention values reported for other immobilised enzyme systems.

The slightly lower response of the immobilised preparation may reflect altered enzyme orientation, partial obstruction of active sites, steric crowding, nanoparticle aggregation, restricted enzyme mobility or external mass-transfer resistance. These factors were not measured independently and are therefore presented only as plausible explanations rather than confirmed mechanisms. Overall, the filter-paper assay demonstrates substantial catalytic functionality of the immobilised preparation under the selected conditions but does not establish a particular binding mechanism, improved stability or industrial performance.

The selected immobilised catalyst loading produced a relatively high filter-paper assay response compared with the selected free-enzyme loading. However, because the preparations were evaluated on different loading bases, the resulting 89% ratio cannot be compared directly with protein-normalised activity-retention values reported for other immobilised cellulase systems. The result demonstrates measurable catalytic functionality of the recovered catalyst but does not quantify the fraction of intrinsic enzyme activity preserved during immobilisation. The difference between free and immobilised cellulase activity could have resulted from several simultaneous effects. Attachment to the nanoparticle surface may have caused minor conformational changes around some enzyme molecules or altered their orientation, potentially reducing active-site accessibility. Some molecules may have been positioned with their catalytic regions facing the particle surface or neighbouring enzymes, creating partial steric hindrance. Nanoparticle aggregation may also have reduced the fraction of surface-associated enzyme that was directly accessible to the filter-paper substrate. In addition, immobilisation restricts enzyme mobility and

may introduce external diffusion or mass-transfer resistance as the insoluble substrate and soluble products move between the bulk reaction medium and the catalyst surface [27].

Conversely, the relatively high retained activity suggests that many of the immobilised enzyme molecules remained in orientations that allowed productive interaction with cellulose. Surface attachment may also have limited extensive unfolding of some enzyme molecules during the assay. Enzyme conformation, orientation and active-site exposure were not directly measured. The result should therefore be interpreted as evidence of substantial functional activity after immobilisation rather than confirmation of a particular molecular mechanism.

Activity-retention values of 30–80% are commonly reported as indicators of successful enzyme immobilisation. High retained activity is often associated with improved operational, thermal and storage stability, making immobilised enzymes more suitable for industrial applications [28]. The 89% relative filter-paper assay achieved in the present work falls within the upper range of values reported for magnetic nanoparticle-based immobilisation systems, indicating that the selected immobilisation strategy effectively enhanced the relative filter-paper assay response. Cellulase immobilised on MnO_2 nanoparticles retained approximately 82% of its original activity following immobilisation [25], while similar studies have reported post-immobilisation activities as high as 90 FPU g^{-1} [29].

3.5. Glucose-Producing Performance of Free and Immobilised Cellulase

The enzymatic hydrolysis of pretreated HH was evaluated over a predefined seven-hour period, with samples collected hourly. Glucose concentration increased progressively for both free and immobilised cellulase, providing a short-term comparison of glucose release under identical experimental conditions. The time-dependent glucose concentrations obtained at a dilution factor of 5 are presented in Figure 4. A dilution factor of 5 was selected as a representative intermediate-to-high enzyme loading that allowed glucose production by both preparations to be monitored throughout the seven-hour period without using the maximum enzyme loading of 2.5; it was not considered an optimised condition. At this dilution factor, free cellulase produced 3.12 g/L glucose after seven hours, while immobilised cellulase produced 2.82 g/L, corresponding to approximately 90% of the glucose produced by the free enzyme. The time-course data were used to describe glucose accumulation over the predefined experimental period and were not interpreted as initial reaction rates or maximum saccharification. These results indicate that the immobilised preparation retained substantial short-term hydrolytic functionality while permitting magnetic catalyst recovery. A comparable study reported hydrolytic efficiencies of 88% for free cellulase and 81% for immobilised cellulase using carboxymethyl cellulose as the substrate [24].

The effect of enzyme dilution on glucose production after seven hours of hydrolysis is presented in Figure 5. At the highest enzyme loading tested, corresponding to a dilution factor of 2.5, free and immobilised cellulase produced seven-hour glucose concentrations of 4.18 and 3.76 g/L, respectively. As the dilution factor increased from 2.5 to 20, glucose concentration decreased from 4.18 to 0.98 g/L for free cellulase and from 3.76 to 0.86 g/L for immobilised cellulase. Across all tested dilution factors, the immobilised preparation generated approximately 88–91% of the glucose produced by the free enzyme. These results demonstrate a consistent enzyme-loading-dependent response for both enzyme preparations, although the comparisons are descriptive and are not interpreted as statistically significant.

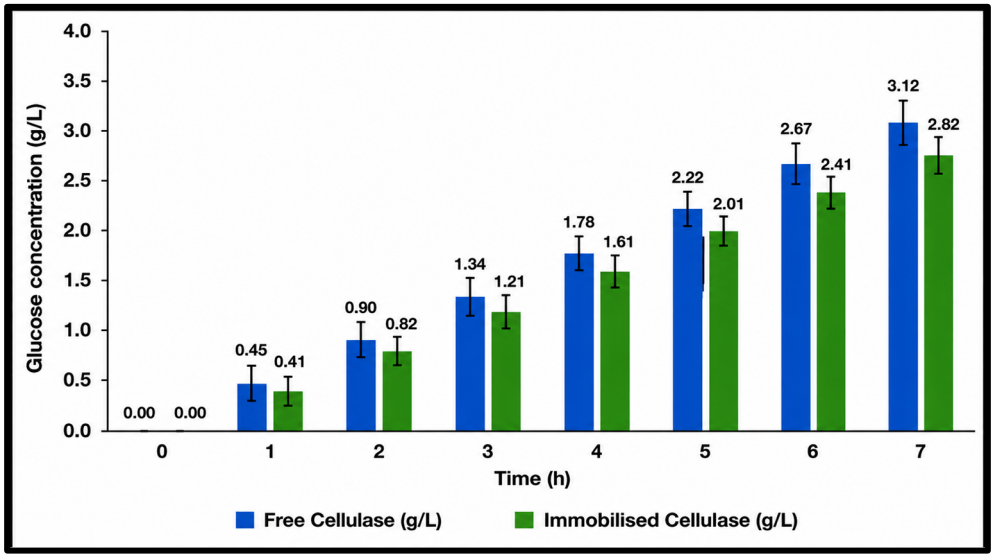

Figure 4. Glucose concentration during the seven-hour hydrolysis of pretreated HH using free and magnetic nanoparticle-immobilised cellulase at a dilution factor of 5. Progressive glucose accumulation was observed for both preparations, while the immobilised cellulase maintained approximately 90% of the glucose-producing performance of the free enzyme. Values represent mean ± standard deviation of three independent experiments (n = 3); error bars indicate standard deviation. Differences between the enzyme preparations are reported descriptively and are not interpreted as statistically significant.

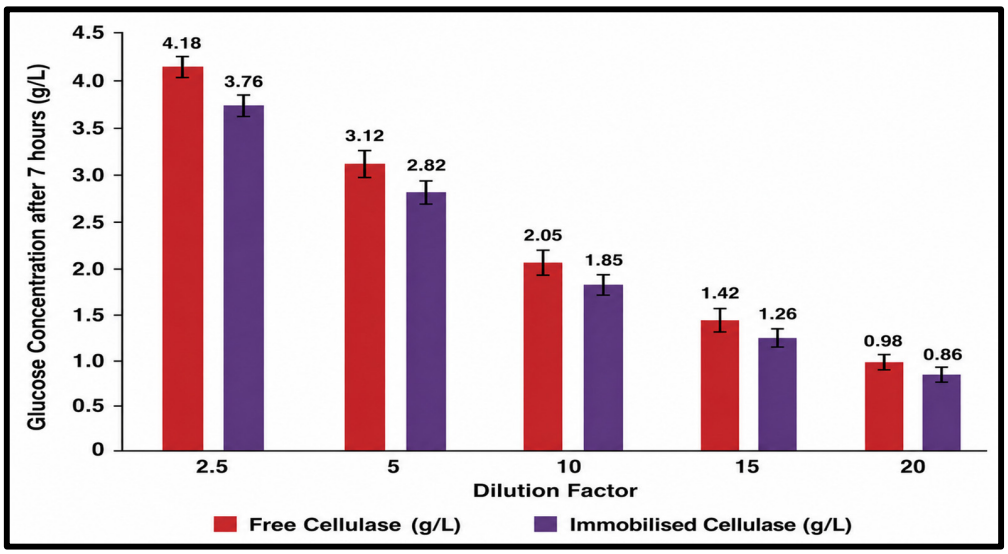

Figure 5. Glucose concentrations obtained after seven hours of hydrolysis of pretreated HH at different free and immobilised cellulase dilution factors. Glucose concentration decreased with increasing enzyme dilution, while the immobilised preparation generated approximately 88–91% of the glucose produced by the free enzyme across the tested dilution factors. Values represent mean ± standard deviation of three independent experiments (n = 3); error bars indicate standard deviation. Comparisons are descriptive and are not interpreted as statistically significant.

To express the seven-hour hydrolysis results relative to the initial biomass and experimentally determined glucan content, the measured glucose concentrations were converted to glucose mass per reaction, glucose yield and glucose-based glucan conversion. The calculated values for free and immobilised cellulase at each enzyme dilution factor are presented in Table 4.

Table 4. Seven-hour glucose yield and glucose-based glucan conversion during hydrolysis of pretreated HH using free and magnetic nanoparticle-immobilised cellulase.

Enzyme Preparation	Dilution Factor	Glucose Concentration at 7 h (g L^{-1})	Glucose Mass per Reaction (g)	Glucose Yield (g g^{-1} Dry Biomass)	Glucose-Based Glucan Conversion (%)
Free cellulase	2.5	4.18 ± 0.14	0.0836 ± 0.0028	0.2090 ± 0.0070	44.2 ± 1.5
Immobilised cellulase	2.5	3.76 ± 0.12	0.0752 ± 0.0024	0.1880 ± 0.0060	39.7 ± 1.3
Free cellulase	5	3.12 ± 0.13	0.0624 ± 0.0026	0.1560 ± 0.0065	33.0 ± 1.4
Immobilised cellulase	5	2.82 ± 0.11	0.0564 ± 0.0022	0.1410 ± 0.0055	29.8 ± 1.2
Free cellulase	10	2.05 ± 0.11	0.0410 ± 0.0022	0.1025 ± 0.0055	21.7 ± 1.2
Immobilised cellulase	10	1.85 ± 0.10	0.0370 ± 0.0020	0.0925 ± 0.0050	19.5 ± 1.1
Free cellulase	15	1.42 ± 0.09	0.0284 ± 0.0018	0.0710 ± 0.0045	15.0 ± 1.0
Immobilised cellulase	15	1.26 ± 0.08	0.0252 ± 0.0016	0.0630 ± 0.0040	13.3 ± 0.8
Free cellulase	20	0.98 ± 0.07	0.0196 ± 0.0014	0.0490 ± 0.0035	10.4 ± 0.7
Immobilised cellulase	20	0.86 ± 0.06	0.0172 ± 0.0012	0.0430 ± 0.0030	9.1 ± 0.6

Values represent mean ± standard deviation from three replicate measurements (n = 3). Calculations were based on 0.400 g dry pretreated HH, a reaction volume of 0.020 L, an experimentally determined glucan content of 42.6% and an anhydro correction factor of 0.90. The reported values represent seven-hour glucose-based conversion and do not constitute complete saccharification or a complete carbohydrate mass balance.

The apparent average glucose release rate decreased as the enzyme dilution factor increased. For free cellulase, the calculated values decreased from 0.60 to 0.14 g/L·h^{-1} as the dilution factor increased from 2.5 to 20. The corresponding values for immobilised cellulase decreased from 0.54 to 0.12 g/L·h^{-1}. These values represent glucose accumulation averaged over the 7 h reaction period and should not be interpreted as initial reaction rates or intrinsic kinetic parameters (Figure 6).

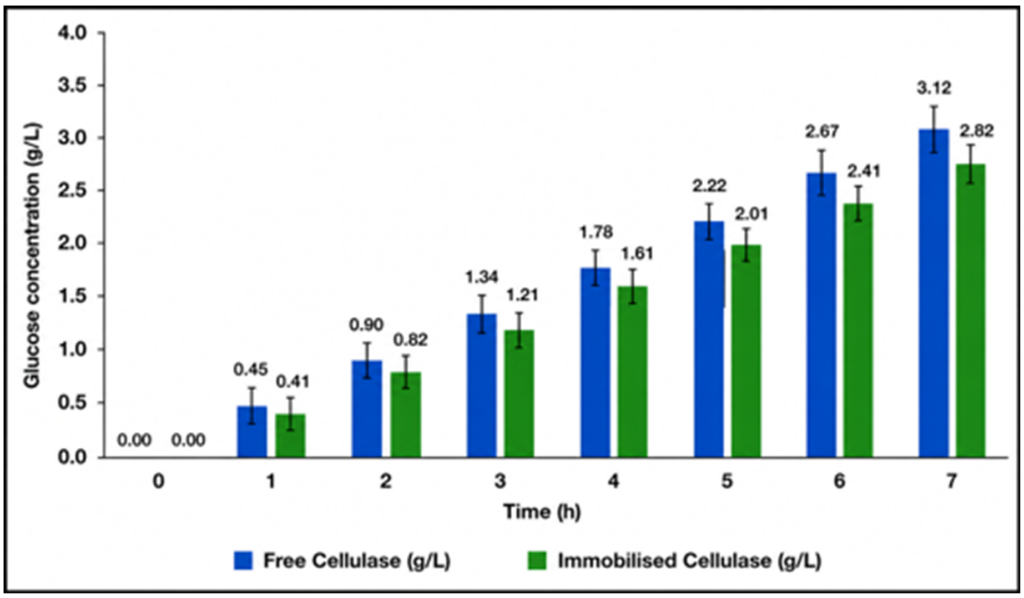

Figure 6. Apparent average glucose release rates for free and magnetic nanoparticle-immobilised cellulase at different enzyme dilution factors. Values were calculated as $C_{7h} - C_{0h}/7$ and decreased with increasing enzyme dilution. The calculated values are descriptive process-performance indicators and do not represent initial reaction rates, kinetic rate constants or Michaelis–Menten parameters. Values represent mean ± standard deviation of three independent experiments (n = 3); error bars indicate standard deviation.

The decreasing values at higher dilution factors are consistent with the reduced quantity of enzyme available for interaction with the pretreated HH substrate. The immobilised preparation showed slightly lower apparent average glucose release rates than the free

enzyme across the tested dilution factors. This difference may reflect several overlapping effects, including restricted enzyme mobility following attachment, partial obstruction of active sites, enzyme orientation on the nanoparticle surface, steric crowding and nanoparticle aggregation. The heterogeneous structure of the hemp hurd substrate may also introduce substrate-diffusion and external mass-transfer limitations by restricting contact between the enzyme-bearing particles and accessible cellulose regions.

The lower apparent average glucose release rates observed for the immobilised enzyme are consistent with diffusion limitations, restricted enzyme mobility on the support surface, steric hindrance effects and potential mass-transfer resistance associated with immobilised biocatalysts [30]. Immobilisation may also influence enzyme orientation on the nanoparticle surface, resulting in partial obstruction of active sites and reduced substrate accessibility [31]. Nonetheless, the comparable concentration-dependent trends indicate that both preparations responded similarly to decreasing enzyme loading. However, the consistently lower values for the immobilised preparation suggest that immobilisation may have introduced moderate accessibility or mass-transfer limitations. The present data do not permit these effects to be quantified individually. The close correspondence between relative activity and glucose release is consistent with retention of catalytic functionality after immobilisation. However, this relationship does not independently identify the mechanisms governing the hydrolysis response.

The calculated values represent apparent average glucose release over the seven-hour hydrolysis period rather than intrinsic enzyme-kinetic rates. Therefore, they cannot be used to estimate K_m, V_{max} or k_{cat}. Reliable determination of K_m and V_{max} would require measurements of initial reaction rates across multiple substrate concentrations under conditions where substrate depletion and product inhibition are minimal. Determination of k_{cat} would additionally require an accurate molar concentration of catalytically active enzyme, which is difficult to define for the commercial multienzyme cellulase preparation used in this study.

The slightly lower apparent average glucose release observed for the immobilised preparation may reflect several overlapping effects, including altered enzyme orientation, partial active-site obstruction, steric crowding, nanoparticle aggregation and mass-transfer limitations. However, these observations cannot be interpreted as changes in substrate affinity or catalytic turnover in the absence of formal kinetic modelling.

3.6. Reusability of Immobilised Cellulase

The short-term reusability of the immobilised cellulase preparation was evaluated over five consecutive hydrolysis cycles using pretreated HH. Glucose production declined progressively across the cycles, with approximately 64% of the initial hydrolytic performance retained by cycle 5, as shown in Table 5.

Table 5. Short-term reusability of immobilised cellulase over five consecutive hydrolysis cycles.

Cycle	Glucose Concentration (g/L)	Residual Hydrolytic Performance (%)
1	2.82 ± 0.09	100 ± 3
2	2.45 ± 0.11	87 ± 4
3	2.10 ± 0.12	74 ± 4
4	1.92 ± 0.13	68 ± 5
5	1.80 ± 0.14	64 ± 5

Values represent mean ± SD (n = 3).

The retention of approximately 64% of the initial hydrolytic performance after five cycles demonstrates short-term magnetic recovery and reuse under the tested laboratory conditions. Enzyme costs remain a major contributor to the overall economics of lignocellu-

losic biomass conversion processes [32,33]. However, this result alone does not establish reduced enzyme consumption, improved process economics or industrial feasibility because catalyst-recovery yield, protein leaching, nanoparticle losses, washing requirements, energy demand and reuse lifetime were not quantified.

Additional activity losses may have resulted from repeated magnetic recovery and washing operations, gradual conformational changes during reuse cycles, or limited enzyme leaching from the nanoparticle surface [25]. Glucose production remained measurable over five consecutive cycles but declined progressively. The results demonstrate short-term recovery and reuse under the tested conditions; they do not establish preservation of enzyme structure, intrinsic catalytic properties or long-term operational stability. A comparable study showed that the immobilised enzyme demonstrated 50% activity retention over five cycles and superior thermostability at 80 °C compared to the free enzyme [24]. Kaur et al. (2021) reported that cellulase immobilised on magnetic nanoparticles retained 50.34% residual activity after four reactions in the enzymatic hydrolysis of rice straw [34].

The five-cycle experiment demonstrates that the cellulase-associated MNP preparation could be magnetically recovered and reused under the tested laboratory conditions while retaining measurable hydrolytic performance. Evaluation of whether this reuse provides an economic or environmental advantage would require measurement of catalyst-recovery efficiency, enzyme leaching, nanoparticle and crosslinker consumption, washing and separation requirements, energy demand, productivity over an extended reuse lifetime and comparison with conventional free-enzyme hydrolysis.

4. Conclusions

The study demonstrated the preparation of catalytically active cellulase-associated amine-functionalised MNPs and evaluated their application in the hydrolysis of pretreated HH. FTIR analysis provided qualitative evidence consistent with cellulase association with nanoparticle preparation, while Bradford protein mass balance quantified the protein retained with the recovered MNPs. These analyses did not establish that the association was exclusively covalent. Under the filter-paper assay conditions, the selected immobilised catalyst loading produced approximately 89% of the total assay response obtained using the selected free-enzyme loading. Because the preparations were compared on different loading bases, this value does not represent protein-normalised activity retention.

Hydrolysis experiments showed a consistent increase in glucose production over the 7 h reaction period for both free and immobilised cellulase. Across all enzyme dilutions investigated, the immobilised cellulase produced between 88 and 91% of the glucose generated by the free enzyme, indicating that immobilisation had only a limited effect on hydrolytic performance. The reported glucose concentrations and cellulose-conversion values represent seven-hour endpoints under the tested laboratory conditions and should not be interpreted as maximum sugar yield, complete saccharification or final glucan conversion. Furthermore, the immobilised cellulase could be magnetically recovered and reused for five consecutive short-term hydrolysis cycles, retaining approximately 64% of its initial hydrolytic performance by the fifth cycle.

Collectively, these findings demonstrate that magnetic nanoparticle immobilisation provides an effective approach for improving cellulase reusability while maintaining hydrolytic efficiency during the conversion of pretreated HHs into glucose-containing hydrolysates. The study represents the third stage of a broader hemp hurd valorisation pathway comprising feedstock characterisation, pretreatment optimisation and enzymatic hydrolysis. The glucose-containing hydrolysates generated in this work provide an important intermediate stream for downstream bioconversion processes. Future research will focus on the in silico engineering and integration of cellulolytic and polyhydroxyalkanoate

biosynthetic pathways to develop consolidated bioprocessing microorganisms capable of simultaneously degrading cellulose and producing PHA/PHB bioplastics. Experimental validation of these engineered systems will contribute towards the development of an integrated hemp hurd biorefinery platform for sustainable bioplastic production.

Author Contributions: Conceptualisation, Z.R.M.; methodology, Z.R.M.; investigation, Z.R.M.; formal analysis, Z.R.M.; writing—original draft preparation, Z.R.M.; writing—review and editing, Z.R.M., S.G., F.D. and N.D.; supervision, F.D. and N.D.; project administration, Z.R.M. All authors have read and agreed to the published version of the manuscript.

Funding: This research received funding for resources from Technology Innovation Agency and Durban University of Technology for processing fund.

Data Availability Statement: The original contributions presented in this study are included in the article. Further inquiries can be directed to the corresponding author.

Acknowledgments: The authors acknowledge the support of the Durban University of Technology and the Technology Innovation Agency in facilitating this research. Further acknowledges the supply of hemp from Department of Agriculture, CEDARA, Pietermaritzburg.

Conflicts of Interest: The authors declare no conflicts of interest.

Abbreviations

ATR	Attenuated Total Reflectance
BCA	Bicinchoninic acid
CMC	Carboxymethyl cellulose
DNS	Dinitrosalicylic acid
DMSO	Dimethyl sulfoxide
FPU	Filter-Paper Unit
FTIR	Fourier Transform Infrared spectroscopy
HH	HH
HPLC	High-Performance Liquid Chromatography
LB	Lignocellulosic biomass
MNP	Magnetic nanoparticle (plural: MNPs)
NaOH	Sodium hydroxide
NHS	N-hydroxysuccinimide
PHA	Polyhydroxyalkanoate
PHB	Polyhydroxybutyrate
SD	Standard deviation
SEM	Scanning Electron Microscopy
Sulfo-SMCC	Sulfosuccinimidyl 4-(N-maleimidomethyl)cyclohexane-1-carboxylate
TGA	Thermogravimetric analysis

References

1. Rajendran, S.; Al-Samydai, A.; Palani, G.; Trilaksana, H.; Sathish, T.; Giri, J.; Saravanan, R.; Lalvani, J.I.J.; Nasri, F. Replacement of Petroleum Based Products With Plant-Based Materials, Green and Sustainable Energy—A Review. *Eng. Rep.* **2025**, *7*, e70108. [CrossRef]
2. Peng, X.; Jiang, Y.; Chen, Z.; Osman, A.I.; Farghali, M.; Rooney, D.W.; Yap, P.-S. Recycling municipal, agricultural and industrial waste into energy, fertilizers, food and construction materials, and economic feasibility: A review. *Environ. Chem. Lett.* **2023**, *21*, 765–801. [CrossRef]
3. Ahmed, A.T.M.F.; Islam, Z.; Mahmud, S.; Sarker, E.; Islam, R. Hemp as a potential raw material toward a sustainable world: A review. *Heliyon* **2022**, *8*, e08753. [CrossRef] [PubMed]
4. Arafat, K.M.Y.; Basak, M.; Agwuncha, S.C.; Mani, K.A.; Bloomquist, M.; Peszlen, I.; Davis, J.; Lucia, L.; Jameel, H.; Pal, L. Optimization of industrial hemp production: Influence of stalk maturity on composition, structure, and processing for sustainable packaging. *Ind. Crops Prod.* **2026**, *243*, 123061. [CrossRef]

5. Przybysz Buzała, K.; Kalinowska, H.; Przybysz, P.; Małachowska, E. Conversion of several types of lignocellulosic biomass to glucose using kraft pulping and enzymatic hydrolysis. *Wood Sci. Technol.* **2017**, *51*, 873–885. [CrossRef]
6. Blasi, A.; Verardi, A.; Lopresto, C.G.; Siciliano, S.; Sangiorgio, P. Lignocellulosic agricultural waste valorization to obtain valuable products: An overview. *Recycling* **2023**, *8*, 61. [CrossRef]
7. Fitzpatrick, M.; Champagne, P.; Cunningham, M.F.; Whitney, R.A. A biorefinery processing perspective: Treatment of lignocellulosic materials to production of value-added products. *Bioresour. Technol.* **2010**, *101*, 8915–8922. [CrossRef] [PubMed]
8. Dos Santos, J.R.; de Souza Moreira, L.R.; Filho, E.X.F. Cellulose-degrading enzymes: Key players in biorefinery development. *Biologia* **2023**, *78*, 1759–1772.
9. Wu, W.; Li, P.; Huang, L.; Wei, Y.; Li, J.; Zhang, L.; Jin, Y. The role of lignin structure on cellulase adsorption and enzymatic hydrolysis. *Biomass* **2023**, *3*, 96–107. [CrossRef]
10. Huang, C.; Li, R.; Tang, W.; Zheng, Y.; Meng, X. Improve enzymatic hydrolysis of lignocellulosic biomass by modifying lignin structure via sulfite pretreatment and using lignin blockers. *Fermentation* **2022**, *8*, 558. [CrossRef]
11. Myeni, Z.R.; Dziike, F.; Motaung, T.E.; Deenadayalu, N. Structural and Chemical Profiling of HH for Sustainable Bioproducts Within a Circular Economy Framework. *Sustainability* **2026**, *18*, 2197. [CrossRef]
12. Myeni, Z.R.; Dziike, F.; Motaung, T.E.; Deenadayalu, N. Low-Concentration Chemical Pretreatment of Lignocellulose Biomass Derived from HH, Agricultural Waste: Comparative Characterisation of Various Pretreatment Methods. *Materials* **2026**, *19*, 843. [CrossRef] [PubMed]
13. Ávila, P.F.; Silva, M.F.; Martins, M.; Goldbeck, R. Cello-oligosaccharides production from lignocellulosic biomass and their emerging prebiotic applications. *World J. Microbiol. Biotechnol.* **2021**, *37*, 73. [CrossRef] [PubMed]
14. Chen, P.; Shrotri, A.; Fukuoka, A. Synthesis of cello-oligosaccharides by depolymerization of cellulose: A review. *Appl. Catal. A Gen.* **2021**, *621*, 118177. [CrossRef]
15. Meng, Q.; Abraham, B.; Hu, J.; Jiang, Y. Cutting-edge advances in strain and process engineering for boosting cellulase production in *Trichoderma reesei*. *Bioresour. Technol.* **2025**, *419*, 132015. [CrossRef] [PubMed]
16. Li, T.; Gong, X.; Yang, G.; Li, Q.; Huang, J.; Zhou, N.; Jia, X. Cross-linked enzyme aggregates (CLEAs) of cellulase with improved catalytic activity, adaptability and reusability. *Bioprocess Biosyst. Eng.* **2022**, *45*, 865–875. [CrossRef] [PubMed]
17. Perwez, M.; Mazumder, J.A.; Sardar, M. Preparation and characterization of reusable magnetic combi-CLEA of cellulase and hemicellulase. *Enzym. Microb. Technol.* **2019**, *131*, 109389. [CrossRef] [PubMed]
18. Budhraja, A.A.; Roy, R. Advancements in cellulase enzyme technology: Applications, challenges, and future perspectives. *Int. Res. J. Mod. Eng. Technol. Sci.* **2024**. [CrossRef]
19. Reshmy, R.; Narisetty, V.; Tarafdar, A.; Bachan, N.; Madhavan, A.; Tiwari, A.; Chaturvedi, P.; Varjani, S.; Sirohi, R.; Kumar, V.; et al. An overview of cellulase immobilization strategies for biofuel production. *BioEnergy Res.* **2023**, *16*, 4–15. [CrossRef]
20. Hassan, M.E.; Zhu, X.; de Souza, E.F.; Elnashar, M.M.; Lu, F.; El-Nashar, M. Enzyme immobilization advances: A key to unlocking renewable bioenergy potential. *Green Chem.* **2025**, *27*, 11289–11311. [CrossRef]
21. Cavalcante, A.L.G.; Dari, D.N.; Aires, F.I.D.S.; de Castro, E.C.; dos Santos, K.M.; dos Santos, J.C.S. Advancements in enzyme immobilization on magnetic nanomaterials: Toward sustainable industrial applications. *RSC Adv.* **2024**, *14*, 17946–17988. [CrossRef] [PubMed]
22. Bilal, M.; Zhao, Y.; Rasheed, T.; Iqbal, H.M.N. Magnetic nanoparticles as versatile carriers for enzymes immobilization: A review. *Int. J. Biol. Macromol.* **2018**, *120*, 2530–2544. [CrossRef] [PubMed]
23. Qin, Y.; Wei, X.; Song, X.; Qu, Y. Engineering endoglucanase II from *Trichoderma reesei* to improve the catalytic efficiency at a higher pH optimum. *J. Biotechnol.* **2008**, *135*, 190–195. [CrossRef] [PubMed]
24. Abraham, R.E.; Verma, M.L.; Barrow, C.J.; Puri, M. Suitability of magnetic nanoparticle immobilised cellulases in enhancing enzymatic saccharification of pretreated hemp biomass. *Biotechnol. Biofuels* **2014**, *7*, 90. [CrossRef] [PubMed]
25. Cherian, E.; Dharmendirakumar, M.; Baskar, G. Immobilization of cellulase onto MnO_2 nanoparticles for bioethanol production by enhanced hydrolysis of agricultural waste. *Chin. J. Catal.* **2015**, *36*, 1223–1229. [CrossRef]
26. Decker, S.R.; Adney, W.S.; Jennings, E.; Vinzant, T.B.; Himmel, M.E. Automated filter paper assay for determination of cellulase activity. *Appl. Biochem. Biotechnol.* **2003**, *107*, 689–703. [CrossRef] [PubMed]
27. Kaur, J. Advanced enzyme immobilization: Problems and solutions. In *Recent Trends in Enzyme Immobilization*; Elsevier: Amsterdam, The Netherlands, 2026; pp. 85–99.
28. Taheri-Kafrani, A.; Kharazmi, S.; Nasrollahzadeh, M.; Soozanipour, A.; Ejeian, F.; Etedali, P.; Mansouri-Tehrani, H.-A.; Razmjou, A.; Yek, S.M.-G.; Varma, R.S. Recent developments in enzyme immobilization technology for high-throughput processing in food industries. *Crit. Rev. Food Sci. Nutr.* **2021**, *61*, 3160–3196. [CrossRef] [PubMed]
29. Yadav, A.; Yadav, D.K.; Rani, P.; Bhardwaj, N.; Gupta, A.; Bishnoi, N.R. Functionalized iron oxide nanoparticles for covalent immobilization of cellic CTec2 cellulase: Enabling enzyme reusability in cellulosic biomass conversion. *Biofuels* **2024**, *15*, 363–373. [CrossRef]

30. Diamanti, E.; López-Gallego, F. Single-Particle and Single-Molecule Characterization of Immobilized Enzymes: A Multiscale Path toward Optimizing Heterogeneous Biocatalysts. *Angew. Chem.* **2024**, *136*, e202319248. [CrossRef]
31. Pagolu, R.; Singh, R.; Shanmugam, R.; Kondaveeti, S.; Patel, S.K.; Kalia, V.C.; Lee, J.-K. Site-directed lysine modification of xylanase for oriented immobilization onto silicon dioxide nanoparticles. *Bioresour. Technol.* **2021**, *331*, 125063. [CrossRef] [PubMed]
32. Abellanas-Perez, P.; Carballares, D.; Rocha-Martin, J.; Fernandez-Lafuente, R. The effects of the chemical modification on immobilized lipase features are affected by the enzyme crowding in the support. *Biotechnol. Prog.* **2024**, *40*, e3394. [CrossRef] [PubMed]
33. Nargotra, P.; Sharma, V.; Lee, Y.-C.; Tsai, Y.-H.; Liu, Y.-C.; Shieh, C.-J.; Tsai, M.-L.; Dong, C.-D.; Kuo, C.-H. Microbial lignocellulolytic enzymes for the effective valorization of lignocellulosic biomass: A review. *Catalysts* **2022**, *13*, 83. [CrossRef]
34. Kaur, P.; Taggar, M.S.; Kalia, A. Characterization of magnetic nanoparticle-immobilized cellulases for enzymatic saccharification of rice straw. *Biomass Convers. Biorefinery* **2021**, *11*, 955–969. [CrossRef]

Disclaimer/Publisher's Note: The statements, opinions and data contained in all publications are solely those of the individual author(s) and contributor(s) and not of MDPI and/or the editor(s). MDPI and/or the editor(s) disclaim responsibility for any injury to people or property resulting from any ideas, methods, instructions or products referred to in the content.